Journal of Cleaner Production 368 (2022) 133104

Contents lists available at ScienceDirect

Journal of Cleaner Production

journal homepage: www.elsevier.com/locate/jclepro

Experimental assessment of thermal and rheological properties of coconut oil-silica as green additives in drilling performance based on minimum quantity of cutting fluids

A.I. Gómez-Merino [a,*], J.J. Jiménez-Galea [b], F.J. Rubio-Hernández [a], I.M. Santos-Ráez [c]

[a] Department of Applied Physics II, University of Málaga, 29071, Málaga, Spain
[b] Department of Civil Engineering, Materials and Manufacturing, University of Málaga, 29071, Málaga, Spain
[c] Department of Mechanical Thermal and Fluids Engineering, University of Málaga, 29071, Málaga, Spain

ARTICLE INFO

Handling Editor: Zhen Leng

Keywords:
Minimum quantity of cutting fluids (MQCF)
Coconut oil
Silica
Latent heat
Thermal conductivity
Viscosity-temperature curve

ABSTRACT

Conventional metal working fluids are prepared from petroleum based mineral oils with toxic, carcinogenic, non-biodegradable and unsustainable additives, which can cause serious environmental contamination and health risks to operators. Formulations with non-toxic emulsifiers and natural additives such as vegetable oils are currently being considered for further development and use of non-toxic tribological products. This study is concerned with the thermal and flow properties of a cutting fluid (taladrine, T) mixed with a phase change material (PCM) coconut oil (CO) in a proportion of 1:9 (CO-0.1T) and hydrophilic silica in 0.01, 0.03 and 0.05 vol fractions. The thermal properties were evaluated by differential scanning calorimetry (DSC) and thermal conductivity measurements while the flow properties were assessed by viscosity temperature curves. The addition of solid particles has demonstrated an enhancement of the thermal conductivities with small differences in the latent heat. The microstructure of the suspensions was established from the DSC cooling dynamic thermogram and the rheological measurements. These results were confirmed by the images of optical polarized microscopy in which plate-like needles were observed. The suspension of 0.03 silica in CO-0.1T demonstrated an adequate gel strength and produced a reduction of 11 °C in drilling performance. A Minimum Quantity of Cutting Fluid (MQCF) of 2 g as an alternative for dry machining and flood cooling. It also prevented evaporative loss and removed metal chips, as a high viscosity complex fluid. In this work the use of phase change materials filled with solid particles as a way of sustainable eco-friendly toxic waste removal in drilling was justified.

1. Introduction

Cutting fluids are coolant and lubricant materials designed specifically for different manufacturing processes. In general, cutting fluids also have anti-corrosion properties, which protect machined surfaces from corrosion. Cutting fluids also save power consumption by reducing machining forces. This is an additional benefit to many industries when electrical demand is reduced (Debnath et al., 2014). The excellent lubricating characteristic of cutting oil facilitates an oil film formation on the workpiece surface and reduce friction coefficient, cutting temperature and cutting forces. It also promotes lubrication, flushing away chips from the machining zone and rust protection. According to the significant performance of oil-based lubricants, there have been numerous studies conducted to enhance their efficiency. Recently, cooling lubricants have included nanoparticles (NPs). The use of nano-additives in the form of NPs is highly efficient due to their high chemical and biological activity. NPs dispersed in a volume of process fluid can easily penetrate between friction surfaces and thereby greatly influence the elastic-hydrodynamic effect of the lubrication. These so-called nano-lubricants has attained much attention in the machining field of manufacturing processes. Researchers have proposed NPs as additives for cutting fluids for various machining processes such as drilling, turning, milling, and broaching, among others. The purposes are reduction of friction and energy consumption, improvement of heat transfer away from the cutting area, more resistance to bacterial or fungi attack, smaller cutting force, lower surface roughness of the workpiece and longer useful life of cutting inserts. For example, SiO_2, TiO_2 (García et al., 2018) and Ag NPs (Bakalova et al., 2017; Sharma et al., 2017) inhibit bacterial growth (respiratory and viability), reduce the average

* Corresponding author.
E-mail addresses: aimerino@uma.es (A.I. Gómez-Merino), j.jimenez@uma.es (J.J. Jiménez-Galea), fjrubio@uma.es (F.J. Rubio-Hernández), imsantos@uma.es (I.M. Santos-Ráez).

https://doi.org/10.1016/j.jclepro.2022.133104
Received 8 March 2022; Received in revised form 21 June 2022; Accepted 9 July 2022
Available online 13 July 2022

Abbreviations

c	Specific heat capacity
CO	Coconut oil
λ	Thermal conductivity
$\varnothing$	Volume fraction
η	Dynamic viscosity
$\dot{\gamma}$	Shear rate
DLS	Dynamic light scattering
DSC	Differential scanning calorimetry
ΔH_{cryst}	Crystallization phase change latent heat
ΔH_{melt}	Melting phase change latent heat
F	Fraction of crystallization
G	Molar activation Gibbs free energy
MQCF	Minimum Quantity Cutting Fluids
MQL	Minimum Quantity Lubrication
n	Index of crystallization
NPs	Nanoparticles
PCM	Phase Change Materials
SEM	Scanning electron microscopy
TEM	Transmission electron microscopy
T	Taladrine
z	Rate constant of crystallization

coefficient of friction (COF) and improve surface roughness. Other particles such as multi-wall carbon nanotubes (MWCN) (Sharma et al., 2019), graphene (Lv et al., 2018; Baldin et al., 2021), graphene with surfactant (Amrita et al., 2019), graphene oxide (Chu et al., 2015), composite, hybrid, or alloys (Singh et al., 2017; Revuru et al., 2017) and NPs of montmorillonite clay are also used (Peña-Parás et al., 2020).

However, conventional metal working fluids are prepared from petroleum based mineral oils with toxic, carcinogenic, non-biodegradable and unsustainable additives, which can cause serious environmental contamination and health risks to operators. Formulations with non-toxic emulsifiers and natural additives are currently being considered for further development and use of non-toxic tribological products (Sen et al., 2021; Gupta et al., 2019). Vegetable oils are biodegradable non-toxic compounds in nature, renewable and environmentally friendly. As major advantages can be mentioned high flash point, high viscosity, high lubricity, superior tribological characteristics than mineral-based oil and low evaporative loss. But their low thermal and oxidative stability, high cost, food versus energy debate and poor cold flow properties are regarded to be the limitations of vegetable oils for their use as base oils for industrial lubricants (Shashidhara and Jayaram, 2010, Kuram et al., 2013). Nevertheless, their properties can be improved by modification, blending, and addition of nanoparticles and ionic liquids. They can be used emulsified as additives in water-based cutting fluids or as metal working fluid in ecological conscious machining to make the process eco-friendly and less toxic for operators (Gajrani and Sankar, 2017). They could also reduce health problems caused by conventional flooding methods used in various machining processes for example drilling, grinding, milling and turning. However, research should concentrate on the solutions to overcome disadvantages and focus on the composition, quantity optimization and recycling of the vegetable-based cutting fluids for green machining. Challenges still exist in achieving sustainability through green manufacturing. A lack of research regarded to the addition of nanoparticles with different surfactants and additives has been reported (Katna et al., 2020).

Metal cutting fluids consume about 16–20% of the entire involved expenses for machining material until the disposal of fluids. Specifically, disposal cost is more expensive than the procured oil. Misuse of the cutting fluid and wrong methods of its disposal can seriously affect human health and the environment. (Sharma et al., 2016). The minimum quantity lubrication (MQL) technology, interpreted as the consumption reduction versus conventional flood cooling procedures, is regarded as a "green" application technology. MQL or MQLCF (minimum quantity of cutting fluids) is a low cost-efficient method of cutting fluid application. It assures the safety for both the environment as well as worker since only small amount of cutting fluid is consumed (Gupta et al., 2020).

The use of MQCF has demonstrated an improvement of the machining performance to be a viable alternative to flooded processes such as drilling. However, use of MQL is limited to mild machining conditions due to high heat generation during machining of hard materials. The applicability of MQL can be extended in aggressive machining conditions by using vegetable-based green cutting fluids (GCF) with solid lubricant nanoparticles as potential additives. Recent nanotechnology developments support innovation needed for transitioning to sustainable production. A nanoparticle-based cooling-lubricating fluid is designed and fabricated by suspending engineered nanoparticles in biodegradable vegetable-based fluid, which enhance their thermal properties for integration into material processing technologies (Krajnik et al., 2016; Gajrani et al., 2019a). Further investigation can also be focussed on the application of MQL/MQCF with nanofluids and hybrid nanofluids in machining of different metals and alloys (Sharma et al., 2016; Gajrani et al., 2019b).

There are many studies concerned with machining performance and tribology. However, fewer research related to thermal properties (thermal conductivity, specific heat capacity, etc.) and especially rheological behavior during the phase change has been carried out. Viscosity and flow rate of the cutting fluids are the factors influencing the capacity in chip removal and the lubrication properties depend upon viscosity (Kuram et al., 2013; Gajrani et al., 2019a). High viscosity cutting fluids could be used differently than conventional flooding methods, for example as a paste, saving a lot of material and reducing temperature. This could be achieved by using phase change fluids as base liquids and nanoparticles as fillers. The aim of this paper is to assess the thermal and flow properties of a cutting fluid composed by 90% of coconut oil and 10% of taladrine with the addition of nano-silica particles in 0.01, 0.03 and 0.05 vol fractions. Both coconut oil and silica particles have shown antimicrobial activity. The addition of nanoparticles to vegetable oils affects the thermal and flow properties of the dispersion. The thermal properties were evaluated by DSC and thermal conductivity. Since coconut oil has a melting point around 20 °C, the phase change is easily achieved in any application. Therefore, changes in the viscosity of suspensions were evaluated through viscosity-temperature curves. Considering the MQCF as "green" technology, the optimum quantity of powder, which produces most satisfactory results with the most suitable flow properties, was also investigated. The main concern was to tailor an eco-friendly cutting fluid, easy to handle and sustainable toxic waste recovery. The better dispersion composition was also tested allowing for its efficiency as a metal working fluid in drilling.

2. Materials and methods

2.1. Materials

Virgin coconut oil (CO) was purchased in a local commercial area. It contains lauric acid (53.70%–54.06%), stearic acid (2.65%–12.10%) and lactic acid bacteria (Lactobacillus plantarum and Lactobacillus paracasei) as main components (Deen et al., 2021). The cutting oil white taladrine (T) was purchased from Quimicrem (Spain). Commercially available Colloidal hydrophilic silica, A200, purchased from Evonik Degussa Ibérica S.A., Spain, (specific surface area BET ≈200 ± 20

m^2/g); density 2.318 7 ± 0.001 2 g/cm^3.

The suspensions were prepared according to the scheme shown in Fig. 1. Coconut oil (CO) was mixed with 10% in volume of the cutting fluid taladrine (CO-0.1T) as liquid phase. Silica powder was added in volume fractions of 0.01, 0.03 and 0.05; the suspensions were stirred in a Onilab OS40-Pro (Labbox-Spain) for 30 min at a rotational frequency of 750 rpm. The samples with different concentration were separated in lots of 35 cm^3 and sonicated at room temperature for approximately 1 h. Afterwards, each sample was allowed to rest overnight before the experimental measurements were recorded.

2.2. Measuring equipment

Micrograph images were carried out on a TEM JEM-1400, JEOL Company, USA. This apparatus is a tungsten-filament 120 kV transmission electron microscope. Samples were dispersed in ethanol, attached to Formvar copper grids by placing one drop on the grid and evaporating the solvent before the images were recorded. Optical images of the crystal morphologies were taken at 20 °C and 40 °C using a polarized microscope with camera (model BX60F/PMC35; Olympus Optical Co., Ltd., Tokyo, Japan). The thermographic images were taken with a Testo, 872 camera (Testo SE & Co. KGaA, Spain). The resolution was 320 × 240 pixels and the thermal sensitivity 0.06 °C.

The powder was weighted using a Mettler AE-163 electronic balance (Mettler-Toledo, Columbus, OH, USA), whose accuracy is 10^{-4} g. The apparent hydrodynamic radius of the particles was obtained by using the Dynamic Light Scattering (DLS) technique on a Zetasizer Nano-S system (Malvern Instruments, UK). This instrument is fitted with Helium–Neon laser source (633 nm and 4.0 mW) and uses a backscattering detection system (scattering angle θ = 173°). It is provided with a built-in Peltier temperature control with an accuracy of ±0.1 °C.

Thermal conductivity measurements were recorded with a KD2 Pro Thermal Properties Analyzer (Decagon Devices, Inc., Pullman, WA, USA) with a maximum error of about 1%, in the temperature range from −10 °C to 85 °C. This device uses the transient hot wire (THW) method to measure thermal conductivity, which minimizes natural convection effects. A volume of 35 cm^3 of the sample was sealed in a glass sample vial (30 mm diameter, 70 mm length). The measurements were carried out with a KS-1 stainless steel thermal probe (1.27 mm diameter, 60 mm length), provided with a heating element and a thermo-resistor, inserted into the sample, as it is described in (Gómez-Merino et al., 2020). The sealed vial was fully immersed in a refrigerated/heating isolated water bath made of stainless steel, with air-cooled refrigerating unit and KISS-Controller model Huber Kiss K6, Germany, equipped with an immersion thermostat. The operating temperature range varied from −25 °C to 200 °C. The uncertainties of thermal conductivities were estimated from standard deviations of experimental data and were lower than 5%.

DSC measurements were recorded in a temperature range from −80 °C to 80 °C at a heat flux of 10 K/min in cooling and 5 K/min in heating into 8 mg of sample. A Mettler Toledo differential scanning calorimeter, DSC 1, (USA) was used. A three-step DSC procedure, involving heating followed by cooling and another heating regime, was followed. The sample was placed in an aluminum pan of 40 μL for 5 min at the initial temperature before the measurements were carried out and another 5 min at the final temperature, with a N_2 flux of 50 mL/min. The DSC measurements were recorded two times from −80 °C to 80 °C and from 150 °C to −80 °C with the same results in the same region. The thermal trace was erased by keeping the sample for 15 min at 80 °C and cooling down to −80 °C. Later, it was kept up to 200 °C for 5 min before starting the heating cycle. The equipment was previously calibrated with In. The latent heat of melting and crystallization, corrected for sample mass (normalized value), expressed in J/g, were calculated from the area under the curve and the base line using the DSC program STARe software 15.01.

Rheological tests were carried out with a Bohlin Gemini controlled stress rheometer (Malvern Panalytical, UK) using a concentric cylinder geometry with a gap of 1 mm. A pre-shear stage was applied to remove the shear history-dependent behavior followed by a resting time before the measurements were recorded. The temperature of the samples was controlled with a Peltier system. Before deciding the shear rate value and heat flux, viscosity-temperature curves at 1, 5, 10, 15 and 30 s-1; 0.5 and 2.5 K/min were carried out. A small shear rate was desirable to correlate the results with the DSC measurements. On the other hand, it was interesting to know the flow properties at the shear rate close to the

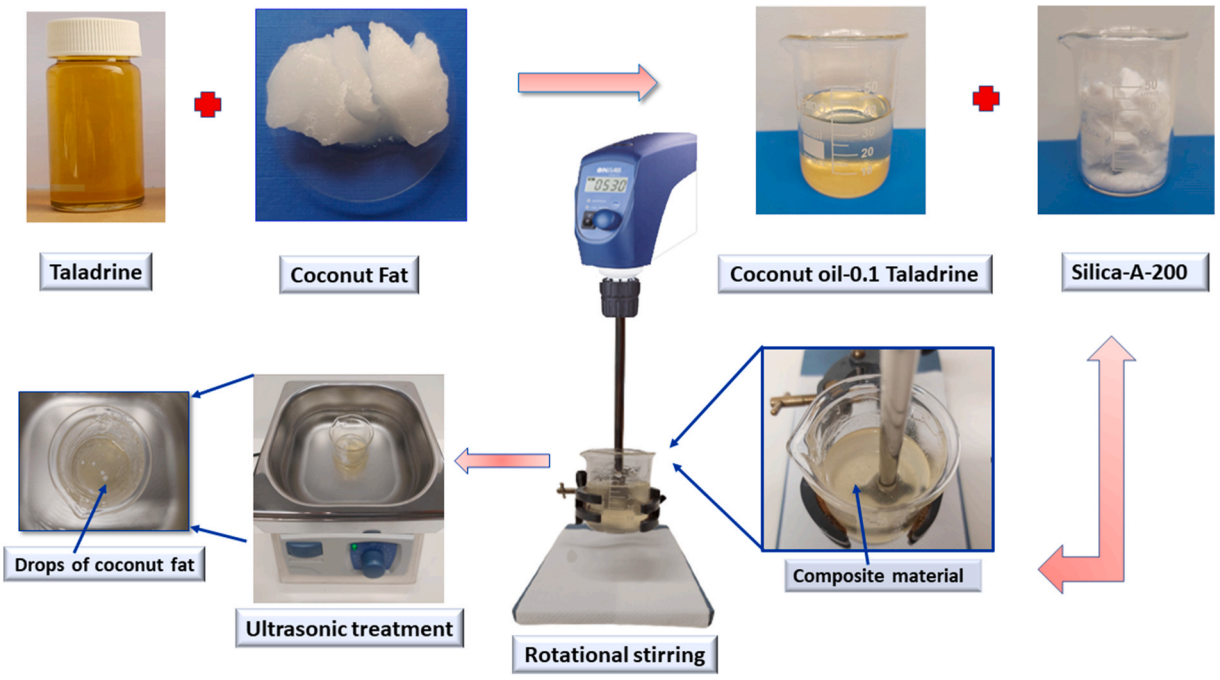

Fig. 1. Scheme of the preparation of the composite samples. CO is mixed with 0.1 vol fraction of the cutting fluid taladrine (CO-0.1T). Silica powder is added in volume fractions of 0.01, 0.03 and 0.05; the suspensions are stirred for 30 min at a rotational frequency of 750 rpm. The samples with different concentration are separated in lots of 35 cm^3 and sonicated at room temperature for approximately 1 h and rest overnight before record the measurements.

drill speed. An estimation of this value at 355 rpm was about 30 s-1. The values over 5 s-1 and 2.5 K/min provided non-reproducible curves and shear rates under 5 s-1 presented high viscosity, which made more difficult to perform the curves. Therefore, the more appropriate values of shear rate and heat flux to record the viscosity-temperature curves were 5 s-1 and 0.5 K/min.

The viscosity-temperature curves were obtained at a constant shear rate of 5 s^{-1} in the interval from 10 °C to 37 °C at a heat flux of 0.5 K/min. The curves were recorded three times and the arithmetical average of the three measurements was considered.

3. Results and discussion

Each type of machining operation requires a specific cutting fluid characterized an adequate thermal and rheological properties and sufficient lubricity. It is desirable a substance with a high viscosity, which results easy to manipulate but also with good thermal properties and low evaporative losses. Gel strength is a crucial property for optimal drilling operations. Excessive gel strength can cause severe drilling problems such as ineffective solids control. Low gel strength values indicate that the fluid will not efficiently suspend the cuttings. An adequate gel strength will allow homogeneous and distributed suspension of the swarf (Vryzas and Kelessidis, 2017). It is ultimately a good compromise of viscosity, thermal conductivity and specific capacity which decide the composition of the cutting fluid (Gajrani et al., 2019b). The use of a phase change cutting fluid enables the gel formation with additives, such as silica, as effective rheology modifier in the appropriate formulation, and thus eliminate the use of other expensive drilling fluid additives. The main concern was the preparation of a minimum quantity of cutting fluid (MQCF) as an alternative for dry drilling or flood cooling with the suitable thermal and rheological properties. The advantage of using a phase change material (PCM) filled with nanoparticles is the benefit of the phase change latent heat exchange, but maintaining the gel microstructure of the suspension, which could be accomplished by adjusting the concentration of silica. At the same time, the material must also be soft enough to be melted for chips and waste recovery and subsequent recycling. The study of the thermal and rheological properties is focused to achieve this target.

3.1. Powder and composite characterization

The transmission electron microscope (TEM) image of A200 silica particles at different magnifications exhibited of spheroidal particles (Fig. 2a), which formed fractal branching structures, as it can be appreciated in Fig. 2b. This results from the irreversible fusion process of the primary pyrogenic particles (Jesionowski and Krysztafkiewicz, 2002). Using the image treatment toolbox of Matlab® (Mathworks, Inc.), an average primary particle size of 10 ± 5 nm was obtained. However, at the microscale, the agglomeration of aggregates could achieve higher effective hydrodynamic particle size when are suspended in a liquid phase. This size was determined by dynamic light scattering (DLS) measurements giving an average value of 330 ± 30 nm for suspensions of A200 silica powder in CO. The addition of 10% taladrine (0.1T) to the CO barely modified the particle size. Fig. 3 shows the pictures of the different samples at 28 °C. It is observed three liquid samples (CO, CO-0.1T, CO-0.1T-0.01 SiO_2 and the more concentrated suspensions (0.03 and 0.05 SiO_2 in CO-0.1T) appear with a gel-like structure even at 28 °C. The corresponding polarized light optical microphotographs of the CO and the composite materials, taken at 20 °C when all the samples are crystallized, are shown below. It can be noticed the stronger microstructure of the two gel-like composite materials, CO-0.1T-0.03SiO_2 and CO-0.1T-0.05SiO_2, compared to the small crystals observed in the other three samples: CO, CO-0.1T and CO-0.1T-0.01SiO_2. This change in the microstructure due to the addition of silica particles also affected the thermal and flow properties, which are analyzed below.

3.2. Thermal properties

3.2.1. Thermal conductivity

Fig. 4a shows the thermal conductivity, λ, of the two fluids, coconut oil (CO), a conventional cutting fluid, white taladrine (T), and the mixture coconut oil-taladrine 0.1 v/v (CO-0.1T) against temperature. It was observed an increase of the thermal conductivity in the phase change in both CO and the mixture CO-0.1T around 20 °C, but under 20 °C the CO-0.1T λ was even lower than those values found in taladrine. At temperatures over the phase change the thermal conductivity progressive and slightly decreased, while these values remained nearly constant along a wide range of temperature in taladrine, with a small decrease at higher temperatures. As it is seen in Fig. 4a, the thermal properties of taladrine improved after mixing with CO, because the amount of CO is much higher. It was unexpected the low thermal conductivity of CO-0.1T at temperatures under 20 °C. The addition of solid particles produced an interesting effect. Fig. 4b describes the effect of the concentration of silica particles A200 on the thermal conductivity in the mixture CO-0.1T. It was also unexpected the low thermal conductivity under 20 °C in 0.03 and 0.05 of silica, as it occurred in CO-0.1T. The effect of the phase change on λ was less evident in the suspensions

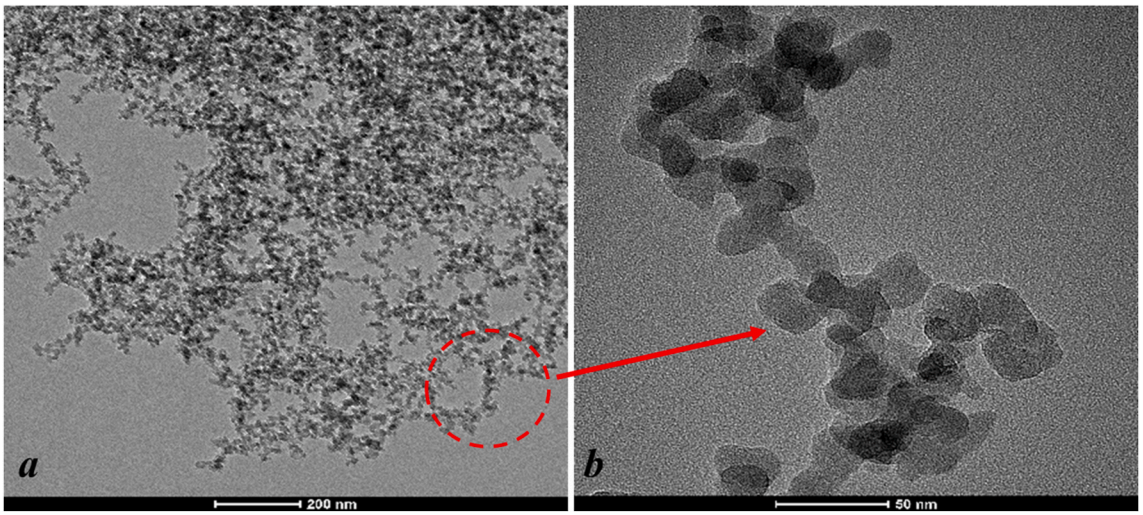

Fig. 2. a) TEM micrography of silica powder showing spheroidal particles. b) Detail of a fractal branching structure formed during the synthesis process.

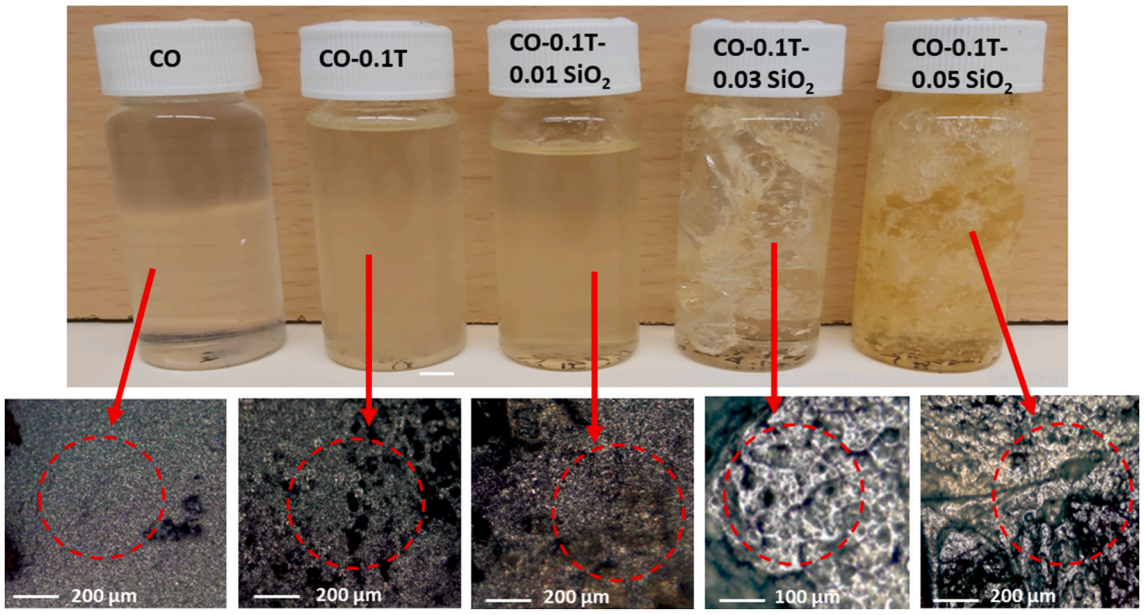

Fig. 3. c) Picture of the liquid phase and the suspensions used in this study at 28 °C. The addition of 0.03 and 0.05 v/v of silica powder form a strong gel-like structure even at 28 °C. The corresponding polarized light optical microphotographs of the CO and composite materials, taken at 20 °C are shown below. Notice the stronger microstructure of the two more concentrated samples compared to the small crystals of the CO, CO-0.1T and CO-0.1T-0.01SiO_2.

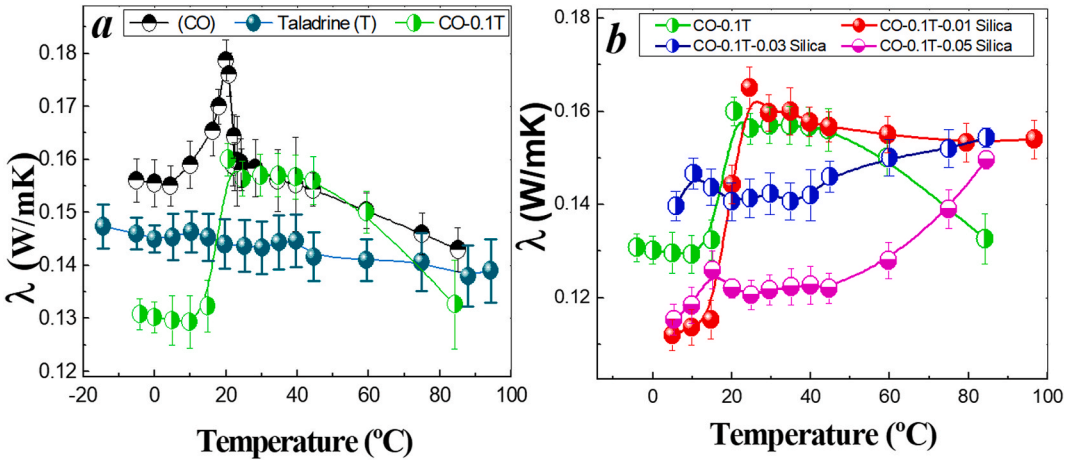

Fig. 4. a) Thermal conductivity vs temperature of CO, Taladrine and CO-0.1T. b) Thermal conductivity vs temperature of 0.01, 0.03 and 0.05 v/v hydrophilic silica A200 in CO-0.1T. In all cases the uncertainties are under 0.01 W/mK.

respect to the base fluid. The thermal conductivity of CO-0.1T-0.01SiO_2 suspensions showed a similar behavior to the liquid phase although this parameter increased over 40 °C being higher than that of CO-0.1T. The more concentrated suspensions, 0.03 and 0.05 SiO_2 revealed an increase of the thermal conductivity with temperature. The phase change in these suspensions, temperatures under 20 °C, was little significant on the thermal conductivity. Probably because only part of the CO melted, and the rest remained occluded in the stronger network formed by the silica particles. In the range between 22 °C and 40 °C, λ was nearly constant and decreased with particle concentration. Over 40 °C λ started a very noticeable increase in all the suspensions being the thermal conductivities at 80 °C very similar for the three concentrations. It could be predictable a higher increase of the thermal conductivity at temperatures over 100 °C. This behavior seemed to be more abrupt at the higher silica concentration 0.05, whose slope is greater (see Fig. 4b). At temperatures under 80 °C, 0.01 and 0.03 SiO_2 were more effective in thermal conductivity enhancement. These values agree with other found in the literature (Silalahi et al., 2021). As it could be expected, the addition of solid particles improved the thermal conductivity of the suspensions at high temperatures, over 80 °C. However, this occurs specially at temperatures over 60 °C. This can be explained due to the influence of the phase change, which is more noticeable at the lowest powder concentration. At higher values, 0.03 and 0.05 SiO_2, the phase change is less evident (see Fig. 3), and λ increased over 60 °C. From Fig. 4b, it can be inferred that the more appropriate concentrations to be used as cutting fluid should be 0.01 or 0.03 SiO_2, depending on the specific heat capacities and the flow properties of both composites.

3.2.2. *DSC analysis*

It has been stated that conduction dominates melting and crystallization processes, although the combination of thermal conduction and natural convection mechanisms are involved in the heat transfer of melting (Yao and Prusa, 1989). A disadvantage of organic phase change materials (PCMs) is their low thermal conductivity. However, sometimes additives may affect the latent heat of phase change (Silalahi et al., 2021). Consequently, enhancing the thermal conductivity of organic

PCMs without causing a major reduction about latent heat is one of the keys to satisfy practical application as latent heat storage/release. The use of nanoparticles as fillers is the most straightforward way to tailor the PCM thermal conductivities and to form additional thermal transport paths within the organic matrix. Silica particles enhanced thermal conductivities of the liquid phase CO-0.1T, as it is shown in Fig. 4b. The corresponding DSC cooling (crystallization) and heating (melting) dynamic thermograms (Fig. 5) of CO and CO-0.1T with the addition of 0.01, 0.03 and 0.05 SiO_2 particles pointed out a phase change in all samples. The crystallization process showed two peaks, reported also by other authors (Srivastava et al., 2017), one of those disappeared at higher silica concentration (>0.03). This change in the DSC is probably due to the different microstructure of the suspensions. Table 1 presents the values of the crystallization and melting of the five samples whose DSC are represented in Fig. 5a. The latent heat of melting and crystallization, corrected for sample mass (normalized value), expressed in J/g, were calculated from the area under the curve and the base line using the DSC program. This table also corroborates small changes in the phase change latent heat respect to that of the liquid phase (CO-0.1T). Besides, thermal conductivity was enhanced specially at 0.01 and 0.03 particle volume fraction (see Fig. 4b). The values for CO agree with other found in the literature (Srivastava et al., 2017).

Fig. 5b describes the dependence of the isobaric specific heat capacity with temperature. The curves were very similar to that obtained in the thermograms of Fig. 5a. The specific capacity is nearly constant with temperature except in the phase change in which raised dramatically. The mechanism underlying the enhancement of Cp in salt-based nanofluids is still not clear and subject of more research (Andreu-Cabedo et al., 2014). Currently, it has been developed a theoretical model in salt-based nanofluids, which suggests the formation of semisolid layering of the salt ions around the nanoparticle surface. The nanoparticles introduced into the salt act as nucleation points for the crystallization of a new phase around them (Shin et al., 2014). This mechanism could also be applied to the CO-0.1T-silica suspensions. The nanoparticles of silica acted as nucleation points for the crystallization of coconut solid phase around them, which usually exhibits higher thermal properties (specific heat capacity and thermal conductivity). The semisolid layering formation ordered around nanoparticles forming fractal-like structures, as it can be seen in Fig. 3, agreed with the increment observed in Cp and the available nanoparticle surface area. The contribution of more experimental work on the mechanism of the heat capacity enhancement of ionanofluids suggests the presence of an interfacial nano layering occurring on the surface of nanoparticles (Oster et al., 2018), which also support the previous model. However, if the semisolid layering become too thick, as occurs in strong gel microstructure, the specific heat capacity could reduce, as it happened in the CO-0.1T-0.05SiO_2. A slight reduction of the suspension specific heat capacity was observed (see Fig. 5b).

As it was mentioned before, the specific heat capacity of coconut oil (CO) presented two peaks, one of these vanished at higher silica concentrations (>0.03). The highest peak was obtained at CO-0.1T-0.01 SiO_2. The process of crystallization might be studied through the Avrami model (Eq. (1)) (Avrami, 1940).

$$(1 - F) = \exp(-zt^n) \tag{1}$$

where F is the fraction of crystallization completed at time t, n is the index of crystallization reaction also named Avrami exponent, and z is the rate constant of crystallization involving nucleation and crystal growth rate, and it depends on the magnitude of n (Kawamura, 1979). The parameter F relates the partial crystallinity defined in terms of partial latent heat, ΔH_t, to the total one achieved, ΔH_{tot}, named as phase change latent heat. It was calculated as $\Delta H_t/\Delta H_{tot}$, where ΔH_t and ΔH_{tot} are the partial and total areas enclosed by the base line and the DSC exothermal peak corresponding to the heat of crystallization, as it is described by Henderson (1979). These values were calculated with the DSC software library. The values of n and z were calculated from the linear form of the Avrami equation (Eq. (3)) as follows:

$$\ln(-ln(1 - F)) = lnz + nln(t) \tag{2}$$

The plot of $ln\ [-ln(1 - F)]$ vs. $ln(t)$ provided the values of n and z calculated from the slope and intercept at ln(t) = 0, respectively. The value of n, the exponent in the Avrami equation, is associated with the mechanisms of crystal growth morphology. In homogeneous nucleation a crystallization process with n = 4 follows a 3-D polyhedral crystal growth mechanism, a value of n = 3 a 2-D plate-like mechanism, and n = 2, linear crystal growth. The adjustment of Eq. (2) to experimental crystallization data are plotted in Fig. 6a. All the curves show more than

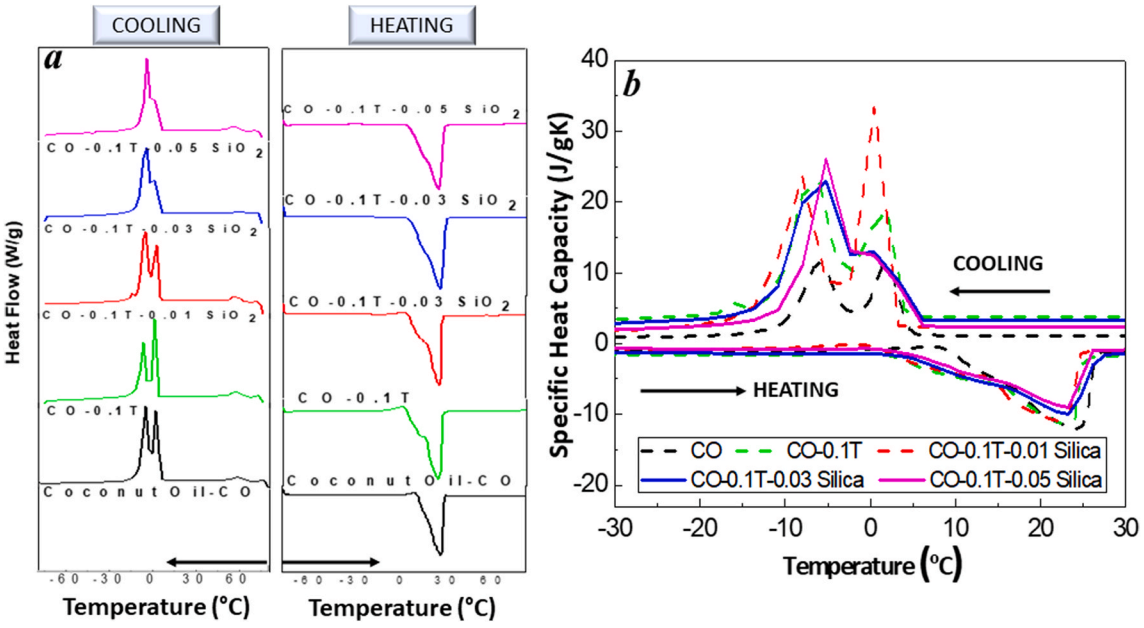

Fig. 5. a) DSC cooling (left) and heating (right) dynamic thermograms of the liquid phases CO, CO-0.1T and the suspensions of 0.01, 0.03, 0.05 v/v of silica in CO-0.1T. The values of the latent heat phase change in melting and crystallization are exhibited in Table 1. In all cases the uncertainties were under 0.001 W/g b) Isobaric specific heat capacity for the five samples: CO, CO-0.1T, CO-0.1T-0.01 silica, CO-0.1T-0.03 SiO_2 and CO-0.1T-0.05 SiO_2.

Table 1
Values of the latent heat of fusion and solidification of the five samples. T_o, onset of the peak, Te, end of the peak, Tc_1, first peak of crystallization, Tc_2, second peak of crystallization, T_C, peak of the crystallization process. All the uncertainties are under 5%.

	ΔH_{cryst} (J/g)	T_o (°C)	T_{c1} (°C)	T_{c2} (°C)	T_e (°C)	ΔH_{melt} (J/g)	T_o (°C)	T_m (°C)	T_e (°C)
CO	97.18	5.96	2.11	−5.74	−16.33	102.44	6.35	24.16	27.15
CO-0.1T	98.83	3.33	0.84	−7.75	−18.33	106.74	12.27	22.52	28.37
CO-0.1T-0.01 SiO_2	94.31	4.12	1.64	−2.87	−15.87	98.85	11.76	22.97	27.12
CO-0.1T-0.03 SiO_2	94.13	5.93	2.31	−16.50	−16.52	101.18	10.53	22.55	28.63
CO-0.1T-0.05 SiO_2	90.68	6.17	5.15	−15.81	−13.67	97.29	13.23	22.58	26.18

one slope. Some authors (Toro-Vazquez et al., 2001) have found in vegetable oils more than one region with different slopes. This change in the slope observed during the process of crystallization is associated with different stages of organization (nucleation, activation, crystal growth and crystal lattice stage) gradually accomplished by the crystals. The crystallization percentage could be represented as a function of crystallization time (Toro-Vázquez et al., 2002). In all the curves exposed in Fig. 6b four different slopes could be distinguished. This figure also shows a tentative representation of the four stages of crystallization, based on the different slopes found in the curves, corroborating this assumption. The longest time was observed in CO-0.1Tand the lowest in CO. The addition of silica helped the crystallization process reducing the time of all the stages respect to the CO-0.1T. Pure CO was able to reach the 100 F faster. The values of n and z for CO, CO-0.1T and the suspensions of silica particles were obtained following Avrami (1940) recommendation fitting the experimental data between the 25 and 75% of crystallization. They are presented in Table 2. From these results, it can be inferred that the addition of taladrine modified the rate constant of crystallization and the crystal morphology. In fact, CO-0.1T showed the highest values of the crystallization index, n, and the lowest crystallization constant rate being less relevant the addition of silica particles. The values of n could change from linear geometry, at the first stages of the crystallization (under 25% of the crystallinity fraction, F) to a plate-like morphology at the later stage. The results of n and z indicated a plate like morphology ($n \sim 3$) except in CO, which is closer to a linear morphology like needles ($n \sim 2$). The adjustment carried out under 25% of crystallization provided lower values of n, which were associated with the initial stages of crystallization (nucleation and activation). Similar results were reported for other authors with several vegetable oils (Toro-Vázquez et al., 2002).

The images of Fig. 7 were recorded with an optical polarized microscope at room temperature. In all pictures, needles of CO are

Table 2
Values of the parameters n and z according to Eq. (2).

	CO	CO-0.1T	CO-0.1T-0.01 SiO_2	CO-0.1T-0.03 SiO_2	CO-0.1T-0.05 SiO_2
n	2.4 ± 0.1	3.0 ± 0.2	2.7 ± 0.1	2.8 ± 0.1	2.7 ± 0.1
z	(1.6 ± 0.8).10^{-6}	(4.5 ± 1.6).10^{-8}	(4.7 ± 1.8).10^{-7}	(8.7 ± 0.5).10^{-8}	(3.2 ± 1.9).10^{-7}
R^2	0.9898	0.9896	0.9793	0.9914	0.9896

observed. This is consistent with n close to 2. As it is seen in Fig. 6a, CO crystalized in shorter time forming entangled needles with $n = 2.4$, Fig. 7a. The addition of 0.1T and silica particles favored the nucleation and activation stages producing clusters of needles with a plate like morphology and n equal to 3 (CO-0.1T) or close to 3 for the silica suspensions. This is clearly observed in Fig. 7b–e. When the samples were warmed at 40 °C the CO melted. The images obtained at 40 °C are shown in Fig. 7f–h. Fig. 7f shows the CO.0.1T-0.01 SiO_2 sample at 40 °C. Only some drops of melted CO are observed. At higher particle concentration part of the CO remained confined in the suspension microstructure. It is clearly seen in Fig. 7g and h, in which the CO is spread among the solid particles. These two images explained the reduction in the phase change latent heat and the specific heat capacity. They also justified why only appeared one peak in the DSC and the specific heat capacity.

3.3. Rheological properties. Viscosity-temperature curves

The rheological behaviour desired for a specific application in machining industries has also to be considered. For this purpose, flow properties were also evaluated. Coconut oil (CO) changes into solid fat around 20 °C at rest and atmospheric pressure. However, if mechanical energy is supplied the phase change conditions can vary. To characterize the flow properties of base fluids and nanofluids viscosity-temperature

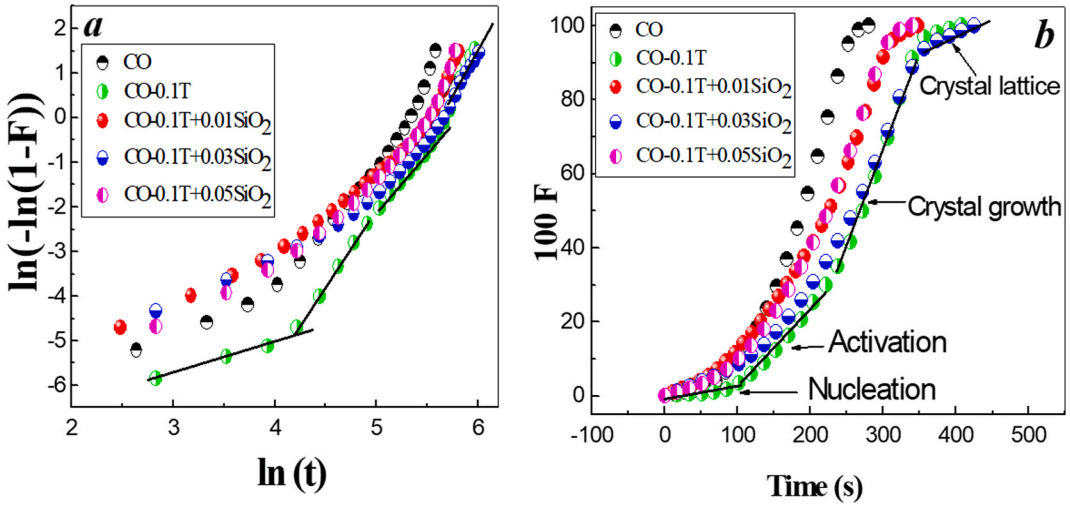

Fig. 6. a) Adjustment of the experimental parameters from the DSC curve according to Eq. (2) for the five samples shown in Fig. 1c, CO, CO-0.1T and the suspensions 0.01, 0.03 and 0.05 v/v of SiO_2 in CO-0.1T. b) Percentage of the crystal transformed at a time t, F, vs time of crystallization. Tentative representation of the four stages of crystallization.

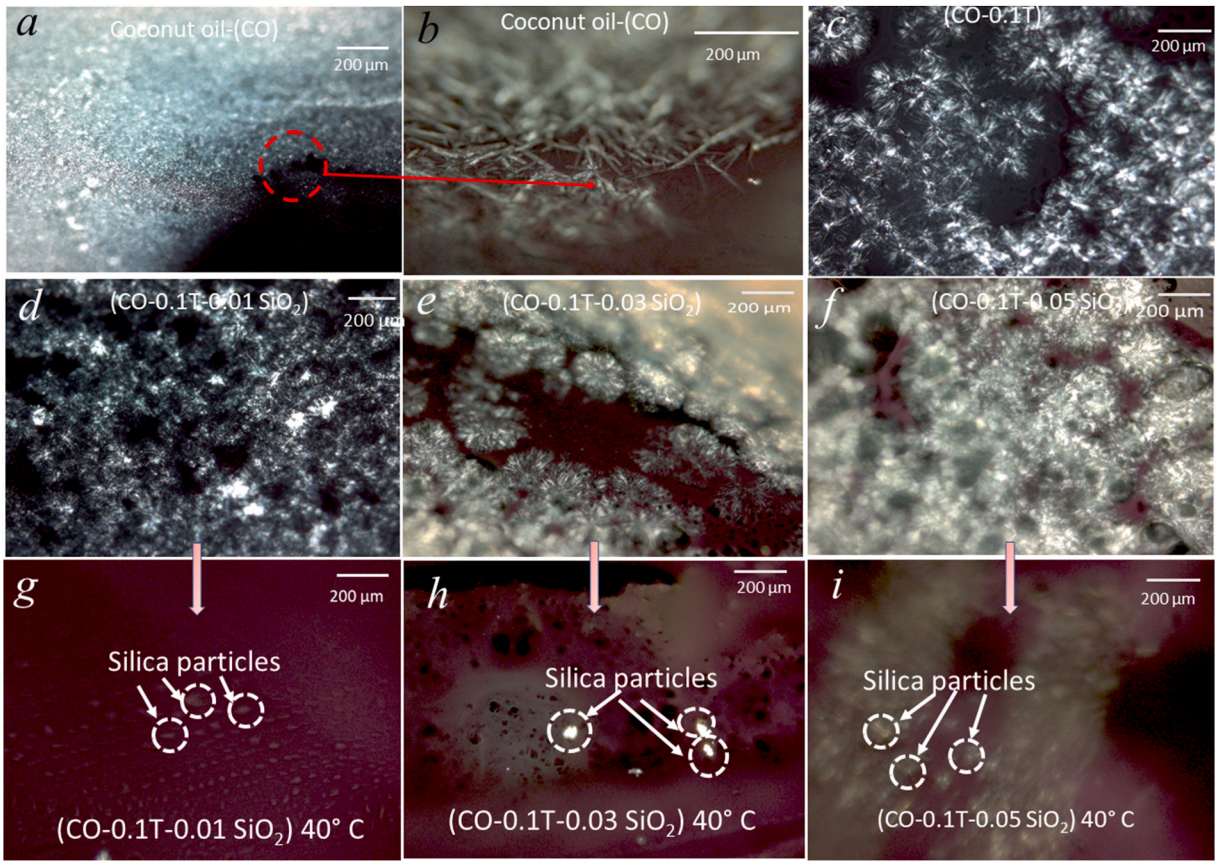

Fig. 7. Polarized light optical microphotographs of a) CO crystals, b) CO-0.1T, c) CO-0.1T-0.01 SiO_2, d) CO-0.1T-0.03 SiO_2 and e) CO-0.1T-0.05 SiO_2. All of them at 20 °C. Images f-h are the samples c, d and e at 40 °C. The red color is a chromatic effect of the camera lens.

curves were recorded in a wide range of temperature.

3.3.1. *Viscosity-temperature curve*

This test consists in a record of viscosity values with a progressive change of temperature, at a constant shear rate. The objective of this experiment was the evaluation of the phase change through the measurement of viscosity. Fig. 8 shows the viscosity vs temperature curves of the CO-0.1T- SiO_2 suspensions, together with the pure taladrine and CO. The curves were performed during the phase change: melting (heating) and crystallization (cooling). In all cases, the shear rate was kept constant at 5 s^{-1}. Since taladrine does not change the phase in the interval of the tested temperature both curves coincided, see Fig. 8a. CO, CO-0.1T and the silica suspensions (0.01, 0.03 and 0.05 of SiO_2 volume fraction in CO-0.1T as liquid phase) (Fig. 8b–f) exhibited a loop for the viscosity curves of melting and crystallization. In all these samples, the melting viscosity curve presented a region in which the viscosity was progressively reducing with temperature. In this zone, it was usually observed an increase-decrease of viscosity probably caused by the inhomogeneities of the phase change. This behavior was more appreciable in the curve of CO (Fig. 8b). The addition of 0.1T and solid particles produced a change in the flow properties increasing the viscosity in all samples. Although the phase change latent heat was nearly the same for all the suspensions (see Table 1). However, the viscosity-temperature curves gave a very interesting information for the CO-0.1T-0.03 SiO_2 and CO-0.1T-0.05 SiO_2. Even though the DSC of these last samples showed a phase change, the consistency of these suspensions behaved as a soft paste or gel, as it is clearly seen in Fig. 3. This was especially evident for CO-0.1T-0.05 SiO_2 suspension, in which the viscosity-temperature loop was very small, Fig. 8f, and the viscosity experimented few changes with temperature because part of the liquid phase remained confined in the gel-like network microstructure. This can be clearly seen in Fig. 8e-f. The activation Gibbs energy increment of the melting and crystallization could be estimated from the well-known Arrhenius equation, used in melt processing optimization of commercial glass (Hrma, 2008):

$$\eta = \eta_\infty exp\left(\frac{\Delta G}{RT}\right) \tag{3}$$

In this expression, η is the viscosity of the suspension, G is the molar activation Gibbs free energy η_∞ is a pre-exponential term corresponding to the viscosity at "infinite" temperature, R the universal gas constant and T the thermodynamic temperature. In general, the pre-exponential factor η_∞ and ΔG depend on shear rate, solid concentration and temperature. Therefore, for given suspensions and constant shear rate here considered, both parameters only would depend on temperature. In the short interval of the phase change, shown in Fig. 8, the Gibbs activation energy was independent of temperature. Consequently, as it can be deduced from Eq. (3), maintaining constant the shear rate (5 s^{-1}) $ln\eta$ of a given suspension linearly depends on temperature inverse (Eq (4)).

$$ln\eta = ln\eta_\infty + \frac{\Delta G}{RT} \tag{4}$$

As it can be observed in Fig. 8 the relationship of lnη vs T in the phase change was certainly linear. Accordingly, lnη vs 1/T was also linear. From the slope the activation Gibbs energy increment was obtained. The results of ΔG are presented in Table 3. The values of the ΔG were calculated in the region where the viscosity changed abruptly because the interval of temperature was smaller, as it can be noticed in Table 3. It is worthy of note that the interval of temperature for the calculation of Gibbs energy was smaller than the phase change temperature interval measured by DSC. In all cases, the activation Gibbs energy was higher in crystallization than in melting. The change of entropy is negative in

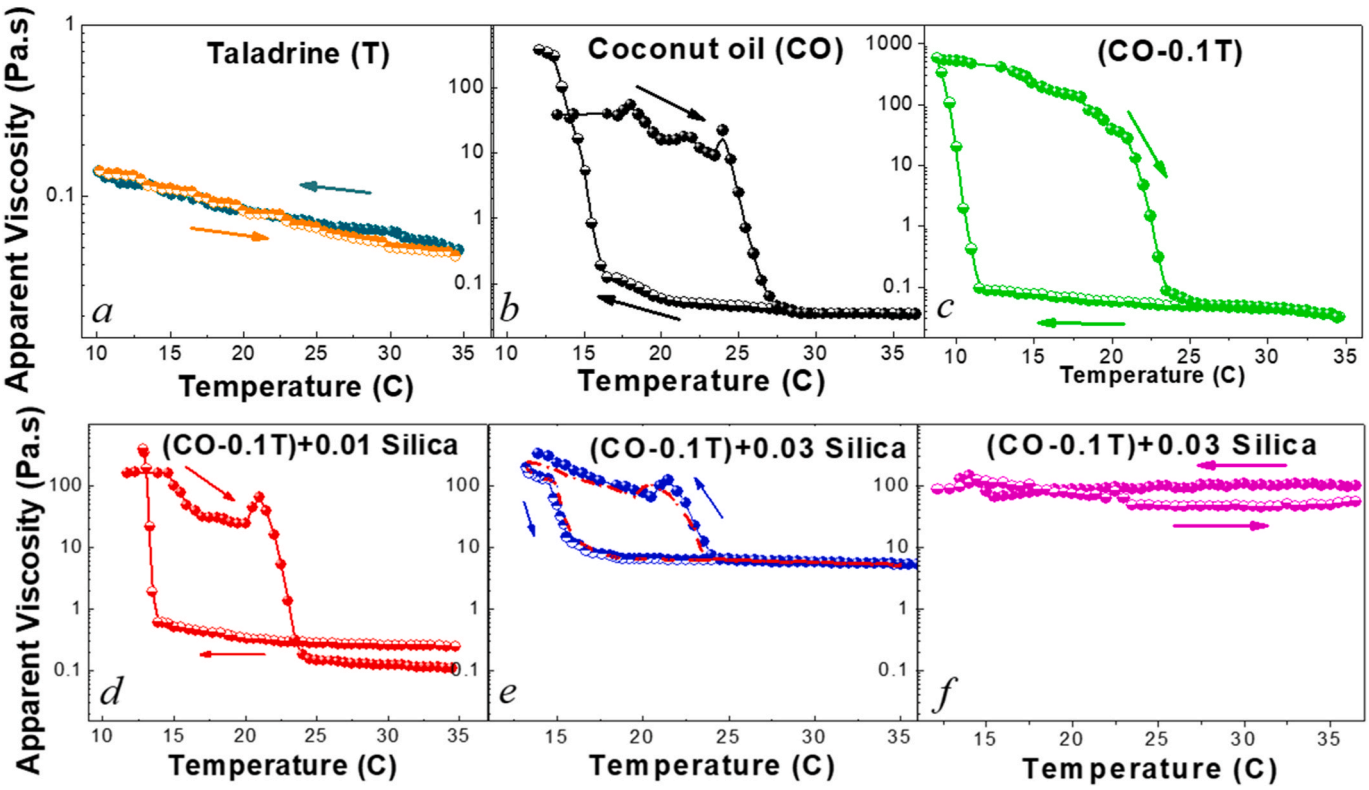

Fig. 8. Viscosity-temperature curves of a) taladrine; b) CO; c) CO-0.1T, and d) CO-0.1T- 0.01 SiO_2; e) CO-0.1T- 0.03 SiO_2, the red curve was obtained after 10 cycles of warming at 100 °C and cooling at 13 °C and f) CO-0.1T- 0.05 SiO_2. The heat flux was 0.5 K/min in melting and crystallization. In all cases the uncertainties were under 0.01 Pas.

Table 3
Values of the Gibbs energy increment and the parameters of Eq. (3) obtained fitting the curves of Fig. 8b–f to Eq. (4). The temperatures T_0-Te indicate the onset and the end of the phase change according to the ramp of temperatures showed in Fig. 6b–f.

	T_0 -T_e (°C)	$\Delta G_{cryst.}$ (kJ/mol)	R^2	T_0 -T_e (°C)	$\Delta G_{melt.}$ (kJ/mol)	R^2
CO	16.1–13.1	1740 ± 20	0.9828	19–22	1440 ± 10	0.9947
CO-0.1T	11.0–8.8	2190 ± 20	0.9885	21–23	1610 ± 15	0.962
CO-0.1T-0.01 SiO_2	13.9–12.9	4750 ± 80	0.9543	22.0–23.5	1890 ± 10	0.9974
CO-0.1T-0.03 SiO_2	15.6–14.8	1290 ± 10	0.9936	22.0–23.5	903 ± 6	0.9947
CO-0.1T-0.05 SiO_2	15.5–14.0	376 ± 5	0.9838	14.5–16.5	67 ± 2	0.8833

crystallization. This may be reflected in a significant activation entropy contribution to the Gibbs energy, which can be expressed as $\Delta G = \Delta H - T\Delta S$. The highest value of the Gibbs energy corresponded to the CO-0.1T-0.01 SiO_2 suspension, which had also the greatest value of the specific heat capacity (see Fig. 5b). But the addition of more silica powder, 0.03 and 0.05, provided suspensions with more solid-like structure. Reasonably, gel-like microstructures are more ordered, and the entropy changes are smaller. In terms of viscosity, it means smaller differences of viscosity during the phase change and lesser numbers of activation Gibbs energy in melting and crystallization, as it can be seen in Table 3. These values appear to be relatively high as compared to others found for vegetable oils, albeit these are obtained from DSC measurements and do not contain suspended particles (Toro-Vazquez et al., 2000; 2002b). By contrast, the values of the pre-exponential factor were very small ($<10^{-30}$). This is because the pre-exponential factor is associated with the viscosity at "infinite" temperature, which is negligible. In the sample of CO-0.1T-0.05 SiO_2 this value increased to 10^{-10} in melting and the Gibbs activation energy reduced two orders of magnitude (67 kJ/mol) in relation to the highest value (1890 kJ/mol) for CO-0.1T-0.01 SiO_2. It is probable that high activation Gibbs energies were associated with solid-like microstructures formed during the phase change.

Compared to the phase change temperature interval obtained by DSC measurements (see Table 1) the viscosity-temperature curves showed the phase change shifted to higher values of temperature. Although the temperature rate was different in DSC (cooling 10 K/min and heating 5 K/min) than in viscosity curves (heating and cooling at 0.5 K/min). However, the main difference was the change in the viscosity of the suspensions 0.03 and 0.05 of SiO_2 powder. Although the difference in the phase change latent heat was not too big (see Table 1) the Gibbs energy increment reduced significatively compared to those values of CO, CO-0.1T and CO.0.1T-0.01 SiO_2. According to the values of the Gibbs activation energy, the suspensions with 0.03 and 0.05 SiO_2 are thermodynamically more stables. The microstructure experimented little variation with the phase change, as it can be observed in Fig. 3. Contrary, the less favorable crystallization was the suspension with 0.01 SiO_2 (ΔG increased). However, the constant rate of crystallization, z, was somewhat greater than that of 0.03 and 0.05 concentrations. It could be explained based on the solid-like microstructure of these suspensions compared to 0.01. The CO melted but the particle network formed with the addition of silica remained strong enough to maintain high consistency even at high temperatures in the samples of 0.03 and 0.05 v/v of SiO_2 in CO-0.1T, see Fig. 8g and h. This not happened with

the 0.01 SiO_2 suspension, see Fig. 5f. It could be taken advantage of the high viscosity of the gel-like 0.03 and 0.05 SiO_2 suspensions in some industrial applications, as it was described below.

3.4. Application to drilling processes

Drilling, as many machining processes, requires the use of cutting fluids for lubricant and heat exchange purposes. As it was said before, another use of PCM should be in drilling works as an alternative of conventional cutting fluids. The CO has already been used as one of the cutting fluids in machining industries (Wickramasinghe et al., 2017; Suvin et al., 2021) because of its thermal and oxidative stability, which is higher than that of other vegetable-based cutting fluids. In this study, the advantage was the high consistency of 0.03 and 0.05 silica in CO-0.1T, which made much easier to handle the paste also facilitating lubrication. The test was carried out with the CO-0.1T-0.03 SiO_2 suspensions because its thermal properties were improved respect to the liquid phase (CO-0.1T) and had more adequate flow properties, i.e., high viscosity. Fig. 9a outlines how the experiment was conducted. An amount of 2 g of CO-0.1T-0.03 SiO_2 was placed on a non-alloy structured steel plate of 0.1 × 0.1 m^2 and 16 mm of thickness, as it is shown in Fig. 9a and the real image in Fig. 9b. The drill was working for 60 s penetrating into the steel leaf, as it is drawn in Fig. 9c. The hole size was 10 mm depth and 5 mm diameter. The drilling machine power was 0.5 kW and the drill speed 355 rpm. The last image was taken 2 min after finishing the drilling process, t = 180 s, as it is shown in Fig. 9d. The temperature was controlled from the beginning with a thermographic camera at intervals of 15 s. The initial temperature of the sample at t = 0 s was 23 °C, as is indicated in Fig. 9e. The final temperature, after 180 s, was 30 °C, Fig. 9f. This protocol was repeated again without cutting fluid (dry drilling). The change of temperature recorded in both cases are presented in Fig. 10. In both cases, the highest value of temperature was reached at 15 s of drilling. The peak of temperature after 15 s was 50 °C with the cutting fluid CO-0.1T-0.03 SiO_2 and 61 °C with dry drilling (see Fig. 10). Then, the heat diffused throughout the steel plate and the temperature descended in both cases. The election of the complex fluid composition was based on the thermal properties (enhancement of the thermal conductivity compared to the liquid phase and good phase change latent heat) but also on the flow properties. A good consistency even at high temperatures was desirable to remove metal chips, see Fig. 9d. Apart from having a good heat exchange high viscosity facilitated a better handle of the fluid. The addition of solid particles in the

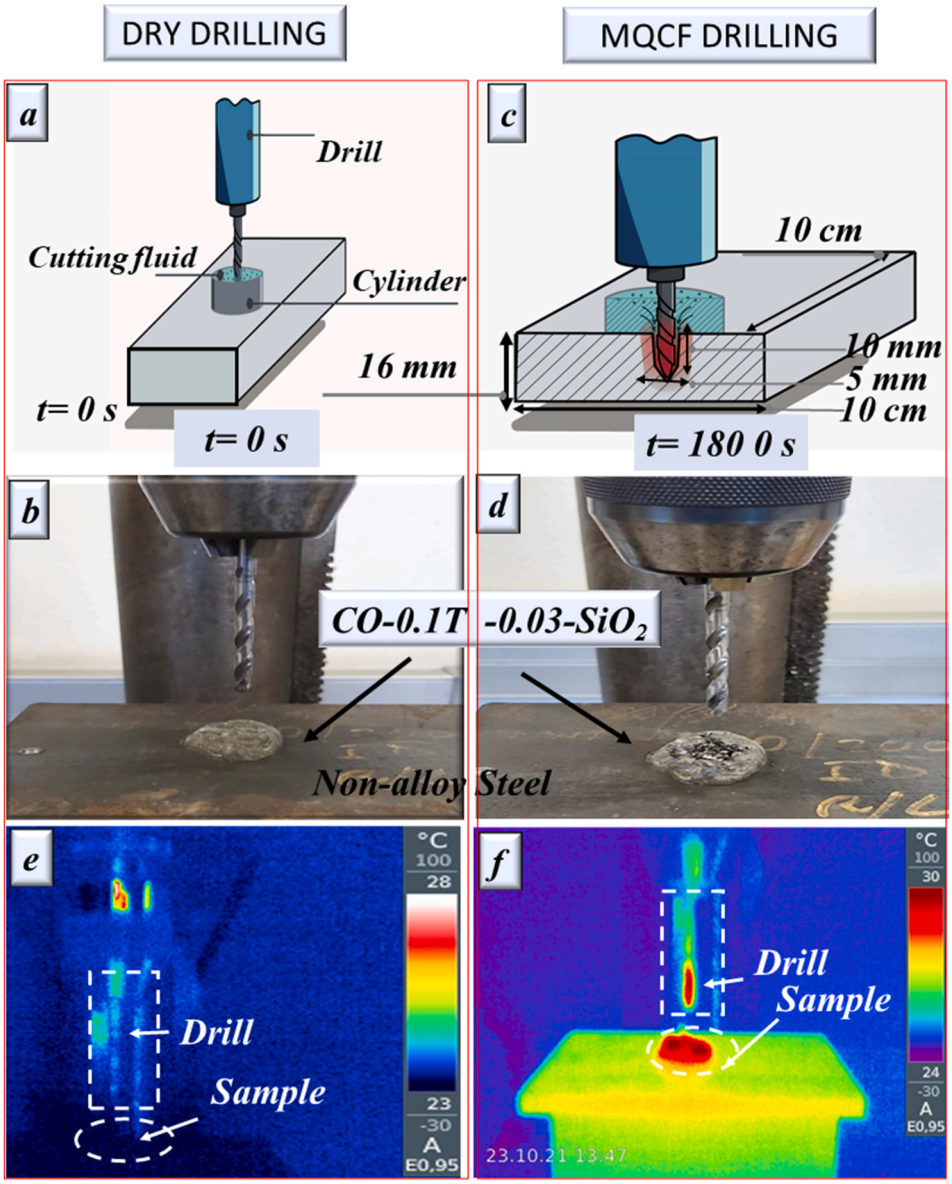

Fig. 9. a) A scheme of the experiment carried out to reduce the temperature in the drilling process using a complex fluid as cutting fluid. b) Real image in which the CO-0.1T-0.03 SiO_2 is placed onto the steel plate at temperature of 23 °C.) c) The complex fluid reduces its viscosity when the temperature increases due to the heat released by drilling and falls into the drill hole. d) Real image showing the metal swarf mixed with the cutting fluid at 180 s, 2 min after drilling. e) Thermal image of picture (b) at the beginning of drilling, t = 0 s. f) Thermal image of picture (d) at 180 s from the start of drilling, the temperature of the fluid in the hole is 30 °C.

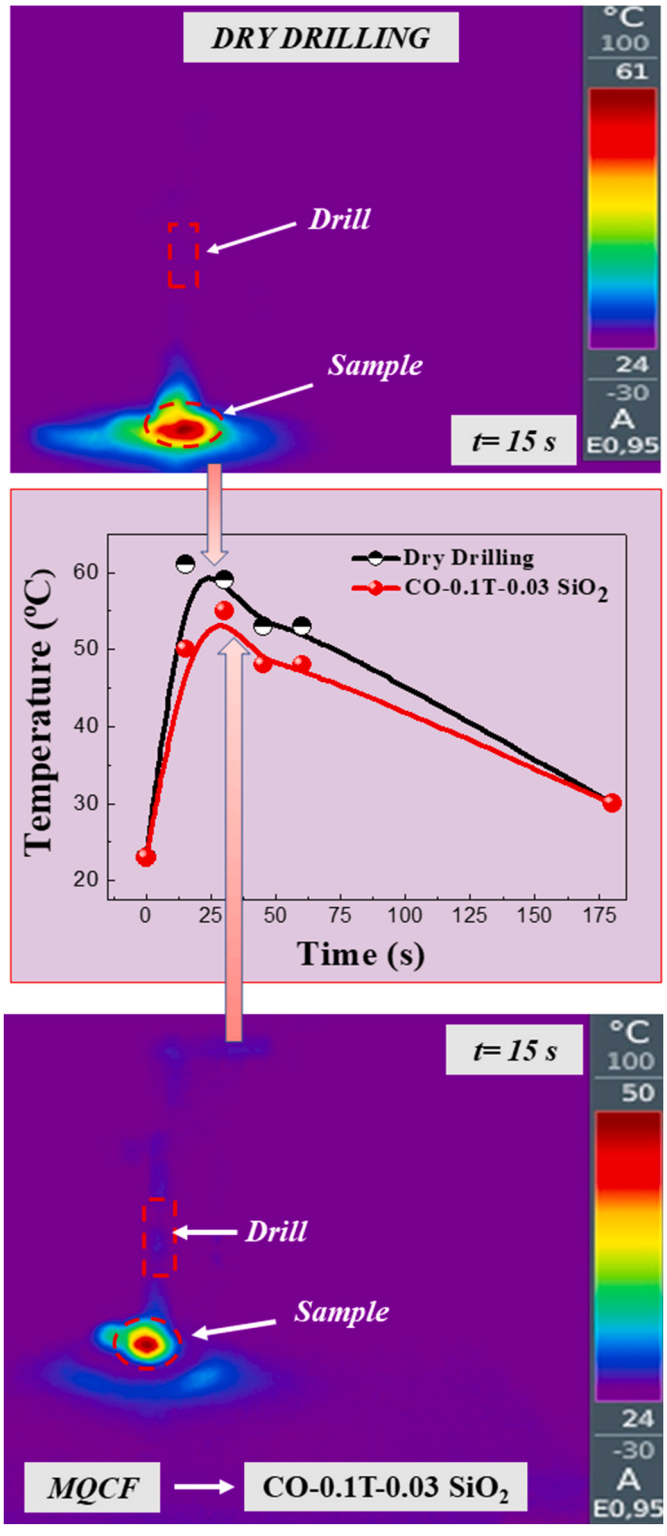

Fig. 10. a) Curves showing the difference of temperatures during drilling with and without cutting fluid. b) Thermal image after 15 s drilling with 2 g of CO-0.1T-0.03 SiO_2 as cutting fluid, with the MQCF technology, the temperature of the sample is 50 °C. c) Thermal image after 15 s of dry drilling, the temperature of the sample is 61 °C.

appropriate concentration produced a kind of gel-like microstructure, which was able to maintain consistent at high temperatures albeit part of the liquid phase was melted. Another important advantage of the use of complex fluids in drilling, a from the removal of heat and metal swarf, was the sustainable waste recovery and the use of MQCF technology, which is environmentally sustainable. The experiment designed for the chip removal and the stability with thermal cycling of the cutting fluid is presented in Fig. 11. It consisted of three cylinders: the extruder, the sieve and the reservoir, which are outlined in Fig. 11a–b. The paste already used was placed into the sieve and it was warmed with the resistance. Then, the extruder was mechanically moved with a crank, and it was falling down into the sieve pressing the fluid with the metal swarf, see Fig. 11c. The metal chips remained in the sieve while the cutting fluid dropped into the reservoir and was left to get colder until room temperature, Fig. 11d. Subsequently, the fluid can be removed from the reservoir and cooled to be reused in another drilling process. Small amount of material (2 g) was able to gather the metal swarf and reduce the steel plate temperature in 11 °C. This aspect is of paramount importance in the environmental sustainability.

The thermal stability was checked by performing three measurements of the thermal conductivity at 25 °C after being heated at 100 °C and cooled at 13 °C for 10 times. It was observed that the measurements were scattered around an average value of 0.141 ± 0.004 W/mK at 24.85 ± 0.03 °C versus the previous value of 0.1413 ± 0.0018 W/mK at 24.73 ± 0.02 °C. The standard deviation of these measurements is below the accuracy given by the KD2 Pro apparatus, showing the thermal stability of the nanofluid.

The viscosity-temperature curve was also recorded three times, after heating at 100 °C and cooling at 13 °C for 10 cycles, from 35 °C to 13.2 °C. The recycling curve is shown in Fig. 8*e* outlined in red dash lines. As an example, the crystallization viscosity in the cooling ramp at 25 °C was 5.859 ± 0.005 Pas, and at 13.8 °C 230.34 ± 0.05 Pas, which supposed a reduction of 5.1% and 0.4% of the former viscosities mean values (6.177 ± 0.003 and 295.35 ± 0.07). During the heating ramp the viscosity at 25 °C was 6.214 ± 0.007 Pas, and at 13.8 °C 295.82 ± 0.05 Pas, which supposed a reduction of 3.3% and 12% of the former viscosities mean values of 6.418 ± 0.003 and 336.35 ± 0.08. Standard deviation of these measurements was in the range of the accuracy given by the rheometer.

In summary, the study of the thermal and flow properties of the coconut oil mixed with 10% of the cutting oil taladrine filled with 0.01, 0.03 and 0.05 v/v of silica was carried out. From this study, the more suitable composition to be used as cutting fluid, considering the principle of minimum quantity of cutting fluid (MQCF), was established as CO+0.1T + 0.03 SiO_2. The quantity of material used was 2 g. This material has exhibited the appropriate gel-like strength to maintain its form during drilling. An experiment was design to carry on waste recovery, as it is shown in Fig. 11.

4. Conclusions

The partial substitution of the metal working fluid taladrine for other eco-friendly phase change vegetable oil, such as CO, has demonstrated to be more effective in the heat exchange. These complex fluids were prepared by adding hydrophilic silica nano-powder to the mixture of CO-0.1T. Suspensions with high viscosities were more useful in drilling metal work than conventional cutting fluids and an alternative to the flooding methods used in various machining processes. CO-0.1T-0.03 silica and CO-0.1T-0.05 silica were able to release part of the CO during the phase change but trapped part of it in its microstructure. As a result, both suspensions exhibited gel-like behavior even at high temperatures over 50–60 °C. They combined the advantage of high latent heat phase change with high viscosity.

The good knowledge of thermal and flow properties was of paramount importance to design the most adequate cutting fluid for a specific machinery process. The viscosity-temperature curves as well as DCS in heating and cooling processes have revealed a good combination to characterize metal work fluids based on eco-friendly phase change materials. The microstructure of the suspensions was established by DSC and rheological measurements. These results were confirmed by the images of polarized light optical microscopy in which plate-like needle

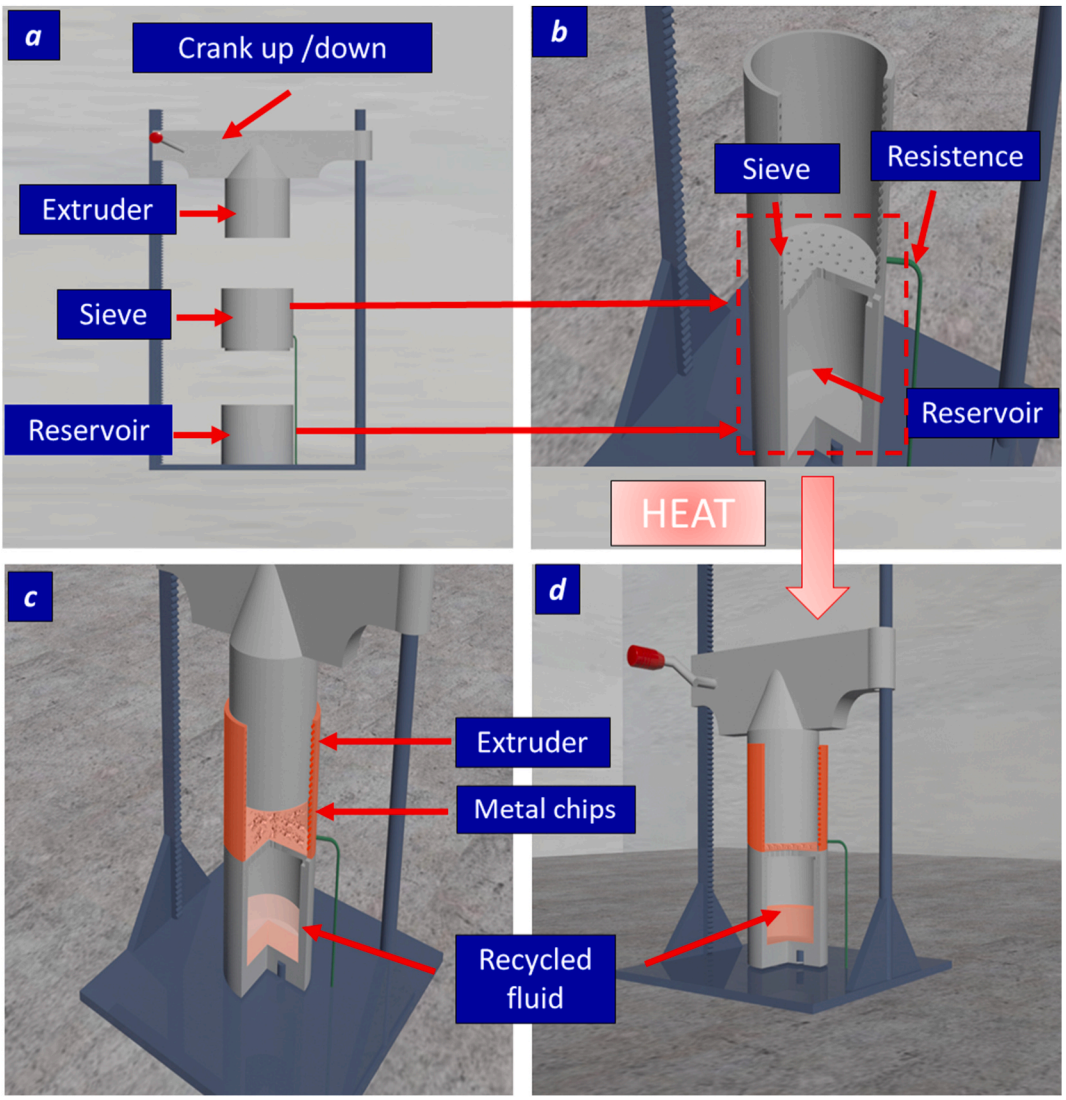

Fig. 11. A scheme of metal chips and cutting fluid recovery. a) the recycler is composed by three cylinders: extruder, sieve and reservoir. b) Inside view of the sieve and the reservoir. c) The resistance starts warming; the extruder falls into the sieve and start pressing the material inside the sieve. d) The metal chips remain inside the sieve and the suspension, less viscous, falls into the reservoir. It is cooled before to be reused again (recycled). Each 10 cycles the thermal conductivity and the viscosity are measured again to check cyclicity.

bunches were observed versus the linear assembling of needles found in the pure CO. The nanoparticles of silica acted as nucleation points for the crystallization of coconut solid phase around them. The semisolid layering formation ordered around nanoparticles forming fractal-like structures agreed with the increment observed in Cp with the addition of silica. To find out more information about the microstructure of the silica particles in CO-0.1T suspensions during the phase change oscillatory tests are suggested as a future work.

An experiment was designed using 2 g of CO-0.1T-0.03 SiO_2 in drilling instead of the conventional flooding method. A reduction of 11 °C was obtained compared to dry drilling. The high viscosity of the cutting fluid, due to its gel strength, allowed the removal of metal swarf and the subsequent recovery of the paste as a melted fluid. The use of these phase change materials filled with solid particles in drilling can reduce the quantity respect to the conventional cutting fluids, what is called MQCF technology, and it is a way of sustainable eco-friendly toxic waste recovery.

Funding

Funding for open access charge: Universidad de Málaga/CBUA.

CRediT authorship contribution statement

A.I. Gómez-Merino: Conceptualization, Methodology, Formal analysis, Resources, Data curation, Writing – original draft, Writing – review & editing, Supervision. **J.J. Jiménez-Galea:** Conceptualization, Methodology, Validation, Investigation, Data curation, Writing – original draft. **F.J. Rubio-Hernández:** Formal analysis, Writing – original draft, Writing – review & editing, All authors have read and agreed to the published version of the manuscript. **I.M. Santos-Ráez:** Validation, Investigation.

Declaration of competing interest

The authors declare that they have no known competing financial interests or personal relationships that could have appeared to influence the work reported in this paper.

Data availability

No data was used for the research described in the article.

Acknowledgments

The authors would like to acknowledge the SCAI service of the University of Málaga for the SEM and TEM images and specially to Dr. A. Arango for kindly recorded the DSC measurements.

References

Amrita, M., Kamesh, B., Srikant, R.R., Prithiviraajan, R.N., Reddy, K.S., 2019. Thermal enhancement of graphene dispersed emulsifier cutting fluid with different surfactants. Mater. Res. Express 6 (12), 125030. https://doi.org/10.1088/2053-1591/ab5517.

Andreu-Cabedo, P., Mondragon, R., Hernandez, L., Martinez-Cuenca, R., Cabedo, L., Julia, J.E., 2014. Increment of specific heat capacity of solar salt with SiO 2 nanoparticles. Nanoscale Res. Lett. 9 (1), 1–11. https://doi.org/10.1186/1556-276X-9-582.

Avrami, M., 1940. Kinetics of phase change. II. Transformation–Time relations for random distribution of Nuclei. J. Chem. Phys. 8, 212–224. https://doi.org/10.1063/1.1750631.

Bakalova, T., Svobodová, L., Rosická, P., Borůvková, K., Voleský, L., Louda, P., 2017. The application potential of SiO_2, TiO_2 or Ag nanoparticles as fillers in machining process fluids. J. Clean. Prod. 142, 2237–2243. https://doi.org/10.1016/j.jclepro.2016.11.054, 2017.

Baldin, V., Rosa Ribeiro da Silva, L., Houck, C.F., Gelamo, R.V., Machado, Á.R., 2021. Effect of graphene addition in cutting fluids applied by MQL in end milling of AISI 1045 steel. Lubricants 9 (7), 70. https://doi.org/10.3390/lubricants9070070.

Chu, B., Singh, E., Samuel, J., Koratkar, N., 2015. Graphene oxide colloidal suspensions as cutting fluids for micromachining—part I: fabrication and performance evaluation. J. Micro Nano-Manuf. 3 (4) https://doi.org/10.1115/1.4031135.

Deen, A., Visvanathan, R., Wickramarachchi, D., Marikkar, N., Nammi, S., Jayawardana, B.C., Liyanage, R., 2021. Chemical composition and health benefits of coconut oil: an overview. J. Sci. Food Agric. 101 (6), 2182–2193. https://doi.org/10.1002/jsfa.10870.

Debnath, S., Reddy, M.M., Yi, Q.S., 2014. Environmental friendly cutting fluids and cooling techniques in machining: a review. J. Clean. Prod. 83, 33–47. https://doi.org/10.1016/j.jclepro.2014.07.071.

Gajrani, K.K., Sankar, M.R., 2017. Past and current status of eco-friendly vegetable oil based metal cutting fluids. Mater. Today Proc. 4 (2), 3786–3795. https://doi.org/10.1016/j.matpr.2017.02.275.

Gajrani, K.K., Suvin, P.S., Kailas, S.V., Mamilla, R.S., 2019a. Thermal, rheological, wettability and hard machining performance of MoS2 and CaF2 based minimum quantity hybrid nano-green cutting fluids. J. Mater. Process. Technol. 266, 125–139. https://doi.org/10.1016/j.jmatprotec.2018.10.036.

Gajrani, K.K., Suvin, P.S., Kailas, S.V., Sankar, M.R., 2019b. Hard machining performance of indigenously developed green cutting fluid using flood cooling and minimum quantity cutting fluid. J. Clean. Prod. 206, 108–123. https://doi.org/10.1016/j.jclepro.2018.09.178.

García, G.E., Trigos, F., Maldonado-Cortés, D., Peña-Parás, L., 2018. Optimization of surface roughness on slitting knives by titanium dioxide nano particles as an additive in grinding lubricant. Int. J. Adv. Manuf. Technol. 96 (9–12), 4111–4121. https://doi.org/10.1007/s00170-018-1834-z.

Gómez-Merino, A.I., Jiménez-Galea, J.J., Rubio-Hernández, F.J., Arjona-Escudero, J.L., Santos-Ráez, I.M., 2020. Heat transfer and rheological behavior of fumed silica nanofluids. Processes 8 (12), 1535. https://doi.org/10.3390/pr8121535.

Gupta, M.K., Jamil, M., Wang, X., Song, Q., Liu, Z., Mia, M., et al., 2019. Performance evaluation of vegetable oil-based nano-cutting fluids in environmentally friendly machining of inconel-800 alloy. Materials 12 (17), 2792. https://doi.org/10.3390/ma12172792.

Gupta, M.K., Mia, M., Jamil, M., Singh, R., Singla, A.K., Song, Q., Liu, Z., Khan, A.M., Rahman, M.A., Sarikaya, M., 2020. Machinability investigations of hardened steel with biodegradable oil-based MQL spray system. Int. J. Adv. Manuf. Technol. 108, 735–748. https://doi.org/10.1007/s00170-020-05477-6.

Henderson, D.W., 1979. Thermal analysis of non-isothermal crystallization kinetics in glass forming liquids. J. Non-Cryst. Solids 30, 301–305. https://doi.org/10.1016/0022-3093(79)90169-8.

Hrma, P., 2008. Arrhenius model for high-temperature glass-viscosity with a constant pre-exponential factor. J. Non-Cryst. Solids 354 (18), 1962–1968. https://doi.org/10.1016/j.jnoncrysol.2007.11.016.

Jesionowski, T., Krysztafkiewicz, A., 2002. Preparation of the hydrophilic/hydrophobic silica particles. Colloids Surf. A Physicochem. Eng. Asp. 207 (1–3), 49–58. https://doi.org/10.1016/S0927-7757(02)00137-1.

Katna, R., Suhaib, M., Agrawal, N., 2020. Nonedible vegetable oil-based cutting fluids for machining processes–a review. Mater. Manuf. Process. 35 (1), 1–32. https://doi.org/10.1080/10426914.2019.1697446.

Kawamura, K., 1979. The DSC thermal analysis of crystallization behavior in palm oil. J. Am. Oil Chem. Soc. 56, 753–758. https://doi.org/10.1007/BF02663056.

Krajnik, P., Rashid, A., Pušavec, F., Remškar, M., Yui, A., Nikkam, N., Toprak, M.S., 2016. Transitioning to sustainable production–part III: developments and possibilities for integration of nanotechnology into material processing technologies. J. Clean. Prod. 112, 1156–1164. https://doi.org/10.1016/j.jclepro.2015.08.064.

Kuram, E., Ozcelik, B., Bayramoglu, M., Demirbas, E., Simsek, B.T., 2013. Optimization of cutting fluids and cutting parameters during end milling by using D-optimal design of experiments. J. Clean. Prod. 42, 159–166. https://doi.org/10.1016/j.jclepro.2012.11.003.

Lv, T., Huang, S., Liu, E., Ma, Y., Xu, X., 2018. Tribological and machining characteristics of an electrostatic minimum quantity lubrication (EMQL) technology using graphene nano-lubricants as cutting fluids. J. Manuf. Process. 34, 225–237. https://doi.org/10.1016/j.jmapro.2018.06.016.

Oster, K., Hardacre, C., Jacquemin, J., Ribeiro, A.P.C., Elsinawi, A., 2018. Understanding the heat capacity enhancement in ionic liquid-based nanofluids (ionanofluids). J. Mol. Liq. 253, 326–339. https://doi.org/10.1016/j.molliq.2018.01.025.

Peña-Parás, L., Maldonado-Cortés, D., Rodríguez-Villalobos, M., Romero-Cantú, A.G., Montemayor, O.E., 2020. Enhancing tool life and reducing power consumption and surface roughness in milling processes by nanolubricants and laser surface texturing. J. Clean. Prod. 253, 119836. https://doi.org/10.1016/j.jclepro.2019.119836.

Revuru, R.S., Posinasetti, N.R., Vsn, V.R., Amrita, M., 2017. Application of cutting fluids in machining of titanium alloys—a review. Int. J. Adv. Manuf. Technol. 91 (5), 2477–2498. https://doi.org/10.1007/s00170-016-9883-7.

Sen, B., Mia, M., Krolczyk, G.M., Mandal, U.K., Mondal, S.P., 2021. Eco-friendly cutting fluids in minimum quantity lubrication assisted machining: a review on the perception of sustainable manufacturing. Int. J. Precis. Eng. Manuf. - Green Technol. 8 (1), 249–280. https://doi.org/10.1007/s40684-019-00158-6.

Sharma, A.K., Tiwari, A.K., Dixit, A.R., Singh, R.K., 2017. Investigation into performance of SiO_2 nanoparticle based cutting fluid in machining process. Mater. Today Proc. 4 (2), 133–141. https://doi.org/10.1016/j.matpr.2017.01.006.

Sharma, A.K., Tiwari, A.K., Dixit, A.R., 2016. Effects of Minimum Quantity Lubrication (MQL) in machining processes using conventional and nanofluid based cutting fluids: a comprehensive review. J. Clean. Prod. 127, 1–18. https://doi.org/10.1016/j.jclepro.2016.03.146.

Sharma, A.K., Katiyar, J.K., Bhaumik, S., Roy, S., 2019. Influence of alumina/MWCNT hybrid nanoparticle additives on tribological properties of lubricants in turning operations. Friction 7 (2), 6. https://doi.org/10.1007/s40544-018-0199-5.

Shashidhara, Y.M., Jayaram, S.R., 2010. Vegetable oils as a potential cutting fluid—an evolution. Tribol. Int. 43 (5–6), 1073–1081. https://doi.org/10.1016/j.triboint.2009.12.065.

Silalahi, A.O., Sutjahja, I.M., Kurnia, D., Wonorahardjo, S., 2021. Measurement studies of thermal conductivity of water and coconut oil with nanoparticles dopant for thermal energy storage, 012022 Int. J. Phys.: Conference Series 1772 (1). IOP Publishing. https://doi:10.1088/1742-6596/1772/1/012022.

Shin, D., Tiznobaik, H., Banerjee, D., 2014. Specific heat mechanism of molten salt nanofluids. Appl. Phys. Lett. 104 (12), 121914 https://doi.org/10.1063/1.4868254.

Singh, R.K., Sharma, A.K., Dixit, A.R., Tiwari, A.K., Pramanik, A., Mandal, A., 2017. Performance evaluation of alumina-graphene hybrid nano-cutting fluid in hard turning. J. Clean. Prod. 162, 830–845. https://doi.org/10.1016/j.jclepro.2017.06.104.

Srivastava, Y., Semwal, A.D., Sajeevkumar, V.A., Sharma, G.K., 2017. Melting, crystallization and storage stability of virgin coconut oil and its blends by differential scanning calorimetry (DSC) and Fourier transform infrared spectroscopy (FTIR). J. Food Sci. Technol. 54 (1), 45–54. https://doi10.1007/s13197-016-2427-1.

Suvin, P.S., Gupta, P., Horng, J.H., Kailas, S.V., 2021. Evaluation of a comprehensive non-toxic, biodegradable and sustainable cutting fluid developed from coconut oil. Proc. Inst. Mech. Eng., Part J: J. eng. tribol. 235 (9), 1842–1850. https://doi.org/10.1177/1350650120975518.

Toro-Vazquez, J.F., Briceno-Montelongo, M., Dibildox-Alvarado, E., Charo-Alonso, M., Reyes-Hernández, J., 2000. Crystallization kinetics of palm stearin in blends with sesame seed oil. J. Am. Oil Chem. Soc. 77 (3), 297–310. https://doi.org/10.1007/s11746-000-0049-x.

Toro-Vazquez, J.F., Dibildox-Alvarado, E., Herrera-Coronado, V., Charó-Alonso, M.A., 2001. Triacylglyceride crystallization in vegetable oils: application of models, measurements, and limitations. In: Widlak, N., Hartel, R., Narine, S.S. (Eds.), Crystallization and Solidification Properties of Lipids. AOCS Press, Champaign, pp. 53–78.

Toro-Vazquez, J.F., Dibildox-Alvarado, E., Charó-Alonso, M., Herrera-Coronado, V., Gómez-Aldapa, C.A., 2002a. The Avrami index and the fractal dimension in vegetable oil crystallization. J. Am. Oil Chem. Soc. 79 (9), 855–866. https://doi.org/10.1007/s11746-002-0570-y.

Toro-Vazquez, J., Herrera-Coronado, V., Dibildox-Alvarado, E., Charo-Alonso, M., Gomez-Aldapa, C., 2002b. Induction time of crystallization in vegetable oils, comparative measurements by differential scanning calorimetry and diffusive light scattering. J. Food Sci. 67 (3), 1057–1064. https://doi.org/10.1111/j.1365-2621.2002.tb09453.x.

Vryzas, Z., Kelessidis, V.C., 2017. Nano-based drilling fluids: a review. Energies 10 (4), 540. https://doi:10.3390/en10040540.

Wickramasinghe, K.C., Perera, G.I.P., Herath, H.M.C.M., 2017. Formulation and performance evaluation of a novel coconut oil–based metalworking fluid. Mater. Manuf. Process. 32 (9), 1026–1033. https://doi.org/10.1080/10426914.2016.1257858.

Yao, L.S., Prusa, 1989. J. Melting and freezing. Adv. Heat Tran. 19, 1–95. https://doi.org/10.1016/S0065-2717(08)70211-9.